The Astronomical Journal, 135:878–891, 2008 March doi:10.1088/0004-6256/135/3/878

THE MASSIVE STAR CONTENT OF NGC 3603*

Nicholas W. Melena[1], Philip Massey[1], Nidia I. Morrell[2], and Amanda M. Zangari[1,3,4]
[1] Lowell Observatory, 1400 W Mars Hill Road, Flagstaff, AZ 86001, USA; nmelena@lowell.edu, Phil.Massey@lowell.edu and azangari@alum.wellesley.edu
[2] Las Campanas Observatory, The Carnegie Observatories, Colina El Pino s/n, Casilla 601, La Serena, Chile; nmorrell@lco.cl
Received 2007 September 18; accepted 2007 December 11; published 2008 February 5

ABSTRACT

We investigate the massive star content of NGC 3603, the closest known giant H II region. We have obtained spectra of 26 stars in the central cluster using the Baade 6.5 m telescope (Magellan I). Of these 26 stars, 16 had no previous spectroscopy. We also obtained photometry of all of the stars with previous or new spectroscopy, primarily using archival *HST* Advanced Camera for Surveys/High-Resolution Camera images. The total number of stars that have been spectroscopically classified in NGC 3603 now stands at 38. The sample is dominated by very early O-type stars (O3); there are also several (previously identified) H-rich WN+abs stars. We derive $E(B-V) = 1.39$, and find that there is very little variation in reddening across the cluster core, in agreement with previous studies. Our spectroscopic parallax is consistent with the kinematic distance only if the ratio of total to selective extinction is anomalously high within the cluster, as argued by Pandey et al. Adopting their reddening, we derive a distance of 7.6 kpc. We discuss the various distance estimates to the cluster, and note that although there has been a wide range of values in the recent literature (6.3–10.1 kpc) there is actually good agreement with the apparent distance modulus of the cluster—the disagreement has been the result of the uncertain reddening correction. We construct our H–R diagram using the apparent distance modulus with a correction for the slight difference in differential reddening from star to star. The resulting H–R diagram reveals that the most massive stars are highly coeval, with an age of 1–2 Myr, and of very high masses (120 $M_{\odot}$). The three stars with Wolf–Rayet features are the most luminous and massive, and are coeval with the non-WRs, in accord with what was found in the R136 cluster. There may be a larger age spread (1–4 Myr) for the lower mass objects (20–40 $M_{\odot}$). Two supergiants (an OC9.7 I and the B1 I star Sher 25) both have an age of about 4 Myr. We compare the stellar content of this cluster to that of R136, finding that the number of very high luminosity ($M_{\rm bol} \leqslant -10$) stars is only about 1.1–2.4× smaller in NGC 3603. The most luminous members in both clusters are H-rich WN+abs stars, basically "Of stars on steroids," relatively unevolved stars whose high luminosities results in high-mass loss rates, and hence spectra that mimic that of evolved WNs. To derive an initial-mass function for the massive stars in NGC 3603 requires considerably more spectroscopy; we estimate from a color–magnitude diagram that less than a third of the stars with masses above 20 $M_{\odot}$ have spectral types known.

Key words: H II regions – ISM: individual (NGC 3603) – stars: early-type – stars: individual (HD 97950) – stars: Wolf–Rayet

1. INTRODUCTION

NGC 3603 is our local giant H II region, and our window into the giant H II regions seen in other galaxies. Its high luminosity was first recognized by Goss & Radhakrishnan (1969). NGC 3603 is located approximately 7–8 kpc from the Sun in the Carina spiral arm. Eisenhauer et al. (1998) estimate that the NGC 3603 cluster has a visual luminosity of 6.1×10^5 $L_{\odot}$, about a factor of 5 lower than that of the R136 cluster in the heart of the giant H II region 30 Doradus in the LMC. The half-light radii are comparable, 4–5 pc (Eisenhauer et al. 1998, and references therein). Its relative proximity allows us a unique opportunity to study the dense stellar cores that are not possible in more distant, unresolved regions. Its stellar content also serves as an interesting comparison to what is known in R136 (e.g., Hunter et al. 1996; Massey & Hunter 1998).

To characterize the massive star population of this high-luminosity H II region requires both photometry and spectroscopy. The first photometric study of NGC 3603 was by Sher (1965), who presented *UBV* photometry (both photoelectric and photographic) for many of the stars in the periphery of the cluster. Sher's (1965) survey was followed by van den Bergh's (1978) photoelectric study, and by Melnick et al. (1989), who used *UBV* CCD images to derive photometry for many of the Sher (1965) stars as well as for some stars located closer to the clusters' core. Melnick et al. (1989) derived a distance of 7.2 kpc, and an age of 2–3 Myr but with evidence of considerable age spread. Moffat et al. (1994) were able to use the *HST* to obtain F439W (essentially *B*-band) photometry of stars even closer to the core, although the images were obtained with the original WF/PC camera and suffered from the effects of the well-known spherical aberration. Near-IR photometry obtained with adaptive optics is discussed by Eisenhauer et al. (1998). Deep *JHKL* photometry extending down to the pre-main-sequence population has been obtained by Stolte et al. (2004), and deep optical photometry has been discussed by Sagar et al. (2001) and Sung & Bessell (2004). Harayama et al. (2008) further explore the low-mass initial mass function (IMF). Pandey et al. (2000) used multi-color photometry to explore the reddening within the cluster, finding that it was anomalously high.

Because of crowding, photometry has been hard enough, but spectroscopy has been all but impossible, especially in the central core. HD 97950, the core of NGC 3603, has been known

* This paper is based on data gathered with the 6.5 m Magellan telescopes located at Las Campanas Observatory, Chile.
[3] Research Experiences for Undergraduates (REU) participant, Summer 2007.
[4] Current address: Wellesley College, 106 Central Street, Wellesley, MA 02481, USA.

to be composite for many years, similar to the situation for R136a in 30 Doradus (see Moffat 1983). It has a collective spectral type of around WN6 + 05 (Walborn 1973). Moffat (1983) classified 13 objects in the cluster with photographic spectra, finding 11 O-type stars, one early B supergiant, plus the unresolved WR core. Some of these spectra were of blends that were not resolved. With the Faint Object Spectrograph (FOS) on the *HST*, Drissen et al. (1995) were able to classify 14 objects, 11 of which were early O-type stars, including five of the earliest class at that time, O3. The spectra of four stars have been modeled: Crowther & Dessart (1998) have analyzed spectra of the three Wolf–Rayet stars in the core, and Smartt et al. (2002) have studied the B supergiant Sher 25.

Here matters have stood until the present. Two of the authors (P.M. and N.I.M.) proposed unsuccessfully several times to obtain spectra of stars in the crowded core of NGC 3603 with the Space Telescope Imaging Spectrograph (STIS) on the *HST*, and after STIS's demise it appeared to many of us that the secrets of NGC 3603 would be well kept for many years to come. However, modern ground-based telescopes now are capable of sub-arcsecond image quality, allowing work from the ground that at one time was only possible from space. Here we utilize the good image quality and large aperture of the Baade 6.5 m telescope for spectroscopy of individual stars inward to the dense central core of NGC 3603, classifying 26 stars, bringing the total number of stars with classification to 38. In addition, we supplement these spectroscopic data with photometry from recently obtained *HST* images. These data permit a better characterization of the massive star population of this nearby giant H II region than has hitherto been possible. In Section 2, we will describe the observations and reductions. In Section 3, we describe our spectral classifications. In Section 4, we will use the resulting spectral types and photometry to derive new values for the reddening and distances to the cluster, and construct an H–R diagram. In Section 5, we will summarize and discuss our results.

2. OBSERVATIONS AND REDUCTIONS

2.1. The Sample

Previous studies have found that the reddening across NGC 3603 is large ($E(B-V) \sim 1.4$) but quite uniform (Moffat 1983), so that the visually brightest stars are likely to have the highest visual absolute magnitudes. Since the cluster is dominated by early O-type stars, optical photometry cannot tell us much about the physical properties of the stars, as the colors are degenerate with effective temperature (see Massey 1998a, 1998b), but does allow one to weed out any obvious non-members as was done by Melnick et al. (1989). Thus we decided to obtain photometry and spectroscopy for as many of the visually brightest members as was practical. To achieve this goal, we identified our sample using *HST* images that had been obtained with the High-Resolution Camera (HRC) of the Advanced Camera for Surveys (ACS) in connection with a different study of NGC 3603.[5] We also use these images for our photometry (Section 2.3).

In Table 1, we list the sample of stars for which we have obtained either spectroscopy or photometry. We were able to obtain photometry for all of the stars with spectroscopy (both our own spectroscopy and previous), and so Table 1 contains all

[5] Obtained under program ID 10602, P.I. = Jesús Maíz Apellániz.

Table 1
NGC 3603 Stars with New Data

Star[a]	α_{2000}	δ_{2000}	V	$B-V$	Spectral Type	Ref.
Sh27	11 15 03.921	−61 15 23.06	15.04	1.05[b]	O7.5 V	1
Sh54	11 15 03.976	−61 15 35.72	14.57	1.08[b]	O6 V	1
103[c]	11 15 06.237	−61 15 36.58	13.09	0.99	O3 V((f))	1
128	11 15 06.422	−61 15 36.42	14.76	0.98	...	...
109[c]	11 15 06.588	−61 15 40.40	13.85	0.99	O7 V	1
Sh50	11 15 06.615	−61 15 23.81	14.70	1.14	...	...
129	11 15 06.685	−61 15 38.85	14.75	0.99	...	...
137	11 15 06.726	−61 15 39.26	14.96	0.99	...	...
111	11 15 06.741	−61 15 35.64	13.87	1.00	...	...
124	11 15 06.815	−61 15 33.95	14.54	1.02	...	...
Sh63	11 15 06.847	−61 15 44.69	13.41	1.04	O3.5 III(f)	1
38[c]	11 15 06.917	−61 15 36.60	13.21	0.97	O4 III(f)	1
45	11 15 06.944	−61 15 38.30	14.14	1.00	O8 V-III	2
37	11 15 07.003	−61 15 37.45	14.16	0.97	O6.5+OB?	2
41	11 15 07.046	−61 15 38.95	14.24	1.00	O4 V	2
42	11 15 07.060	−61 15 39.30	12.99	1.03	O3 III(f*)	2
101	11 15 07.068	−61 15 45.32	14.02	1.08	O6.5 V((f))	1
36	11 15 07.078	−61 15 37.56	14.52	0.99	O6 V	2
40	11 15 07.124	−61 15 39.09	13.33	1.05	O3 V	2
Sh53	11 15 07.148	−61 15 54.86	14.47	1.12[b]	O8.5 V	1
120	11 15 07.211	−61 15 41.50	14.35	1.03	...	...
104	11 15 07.279	−61 15 34.94	13.02	1.06	O3 III(f)	1
A1	11 15 07.305	−61 15 38.43	11.18	1.03	WN6+abs	2
A2	11 15 07.313	−61 15 38.79	12.53	1.04	O3 V	2
A3	11 15 07.352	−61 15 38.46	13.09	1.04	O3 III(f*)	2
33[d]	11 15 07.363	−61 15 39.54	13.69	1.03	O5 V+OB?	2
B	11 15 07.411	−61 15 38.58	11.33	1.01	WN6+abs	2
Sh56	11 15 07.498	−61 15 46.35	13.48	1.08	O3 III(f)+O?	1
C	11 15 07.589	−61 15 38.00	11.89	1.05	WN6+abs	1
139	11 15 07.591	−61 15 32.64	14.88	1.08	...	...
116	11 15 07.593	−61 15 35.96	14.10	1.04	...	...
117	11 15 07.623	−61 15 30.24	14.17	1.10	O6 V	1
125	11 15 07.630	−61 15 31.35	14.50	1.06	...	...
Sh25	11 15 07.649	−61 15 17.59	12.23	1.42[b]	B1 Iab	1
141	11 15 07.692	−61 15 34.65	15.02	1.04	...	...
Sh64	11 15 07.822	−61 15 27.93	13.58	1.15	O3 V((f))	1
16	11 15 07.825	−61 15 37.84	13.53	1.08	O3 V	2
102	11 15 08.073	−61 15 34.24	15.32	1.10	O8.5 V	1
135	11 15 08.106	−61 15 40.30	14.75	1.06	...	...
Sh57	11 15 08.198	−61 15 47.33	13.28	1.06[b]	O3 III(f)	1
108[c]	11 15 08.513	−61 15 38.30	13.71	1.10	O5.5 V	1
Sh18	11 15 08.712	−61 15 59.95	12.65	1.21[b]	O3.5 If	1
Sh58[c]	11 15 08.699	−61 15 44.49	14.24	...	O8 V[e]	1
Sh24	11 15 08.905	−61 15 27.32	14.27	1.11[b]	O6 V	1
Sh49	11 15 09.129	−61 15 33.18	14.67	1.10[b]	O7.5 V	1
Sh47	11 15 09.353	−61 16 02.07	12.72	1.14[b]	O4 V	1
Sh23	11 15 09.849	−61 15 30.48	12.70	1.14[b]	OC9.7 Ia	1
Sh22	11 15 10.071	−61 15 38.01	13.21	1.06[b]	O3 III(f)	1
Sh21	11 15 11.074	−61 15 36.85	14.75	1.12[b]	O6 V((f))	1
Sh19	11 15 11.317	−61 15 55.63	13.65	1.02[b]	O3 V((f))	1

Notes.
Units of right ascension are hours, minutes, and seconds, and units of declination are degrees, arcminutes, and arcseconds.
[a] Nomenclature: stars with "Sh" designations are from Sher (1965). Stars with two digits are from Moffat et al. (1994), and are re-identified in Drissen et al. (1995) as "*HST*-nn." The "A," "B," and "C" components in the central core are from Drissen et al. (1995). The three-digit numbers are from the present paper.
[b] $B-V$ values from Melnick et al. (1989).
[c] Slightly blended on slit.
[d] Blended on ACS image.
[e] Composite?
References. For spectral types: (1) this paper; (2) Drissen et al. (1995).

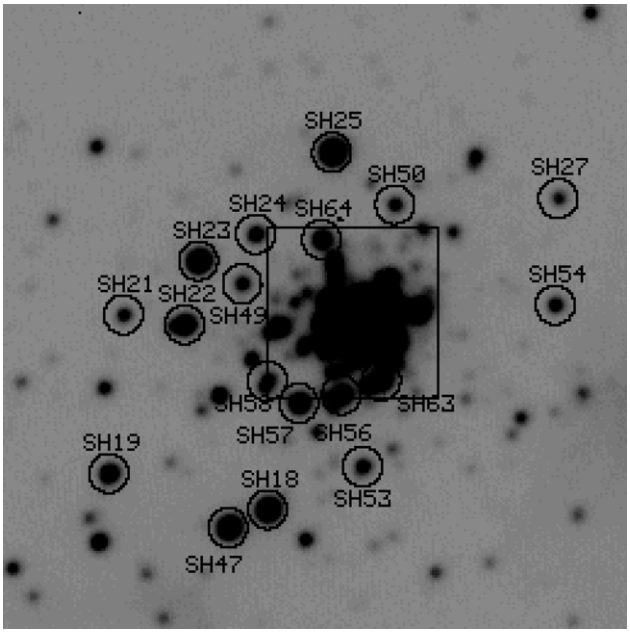

Figure 1. Finding chart for stars in our sample from the periphery of NGC 3603. The field of view is about 1′.0 on a side. North is up, and east is to the left. The chart is made from a *V*-band image taken with the CTIO Yale 1.0 m telescope. The circles are 4″.6 in diameter, or 0.17 pc at an assumed distance of 7.6 kpc. The square denotes the approximate area shown in Figure 2.

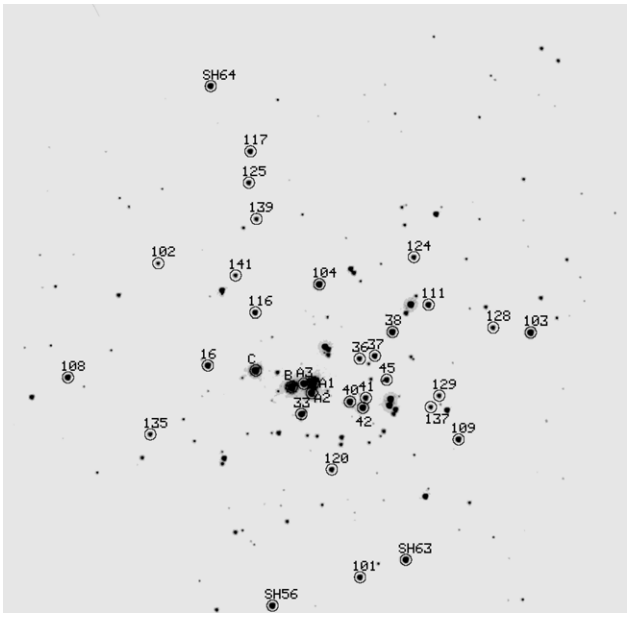

Figure 2. Finding chart for stars in our sample from the center of NGC 3603. The field of view is 20″ on a side, and roughly corresponds to the square outline shown in Figure 1. The image has been rotated so that north is up and east is to the left. The chart was made from a *V*-band ACS/HRC image. The circles are 0″.4 in diameter, or 0.02 pc at an assumed distance of 7.6 kpc.

of the NGC 3603 stars with optical spectroscopy to the present.[6] Of these, 26 were obtained by ourselves in the present study. We have included a few stars with new photometry for which we lack spectroscopy as yet. The coordinates in Table 1 have been determined from the ACS images and our own ground-based images, where care has been taken to place these on the UCAC2 system (Zacharias et al. 2004). We have retained previous nomenclature for stars with previously published spectroscopy or for stars clearly identified in Sher (1965), but difficulties in identification from the finding charts published by Melnick et al. (1989) and Moffat et al. (1994) have resulted in our presenting new designation for other stars. All stars in our sample are identified in Figures 1 and 2.

2.2. *Spectroscopy*

Optical spectroscopy was obtained by N.I.M. during two nights with the Baade 6.5 m Magellan telescope on Las Campanas: 2006 April 12 and 15. The data were taken with the Inamori Magellan Areal Camera and Spectrograph (IMACS) in its long camera mode ($f/4$) using the 600 line mm^{-1} grating. The wavelength coverage was approximately 3600–6700 Å, with a dispersion of 0.37 Å pixel^{-1}, and a spectral resolution of 2.0 Å. The detector for IMACS consists of a mosaic of eight CCDs. In our case, the spectra fell only along one row of four CCDs, and the camera was oriented such that the dispersion crossed all four CCDs, leaving three narrow (20 Å) gaps in our coverage: 4330–4350 Å (which included Hγ), 5120–5140 Å, and 5920–5940 Å. A long 0″.7 slit was used.

The spectrograph was usually rotated so that we would obtain two or more stars of interest on the slit at the same time. A direct image was usually obtained immediately before the spectroscopic exposure, allowing us to be quite certain of the identification of stars for which we obtained data, including those that were coincidentally observed by their falling by chance on the slit. Flat-field exposures were obtained at the beginning and/or end of each night, and He–Ne–Ar comparison arc exposures were taken for each new position. The spectroscopic exposures typically consisted of three individual exposures in order to facilitate the removal of cosmic rays. Exposure times ranged from 3 × 250 s to 3 × 600 s.

The seeing was good but not spectacular. Using the direct images we obtained adjacent to the spectroscopic exposures, we measured an average full width at half maximum of 0″.9 on the first night, and 0″.8 on the second. The best images were 0″.67, and the worst were 1″.1.

Each chip and exposure were reduced separately, and the data were combined at the end to produce a single spectrum for each object along the slit. The processing steps were the usual ones and were done using IRAF.[7] First, the overscan was used to remove the bias on each chip, and then the two-dimensional bias structure was subtracted using the average of ten zero-second exposures. The flat-field exposures were divided into the data, after normalization. The spectra were extracted using an optimal extraction algorithm, after defining the location of stars of interest and selecting the sky background regions interactively. The same trace (spatial position as a function of wavelength) and extraction apertures were then applied to the comparison arcs, and a wavelength solution was found for each aperture. The stellar spectra were then normalized to the continua, combined, and the four wavelength regions merged into a single spectrum for each star.

[6] This excludes the Moffat (1983) spectra of blobs given letter designations.

[7] IRAF is distributed by the National Optical Astronomy Observatories, which are operated by the Association of Universities for Research in Astronomy, Inc., under cooperative agreement with the National Science Foundation (NSF). We are grateful to the on-going support of IRAF and the help "desk" maintained by the volunteers at http://www.iraf.net.

The typical signal-to-noise ratio (SNR) is 200–500 per 2 Å spectral resolution element. Such good quality spectra are essential for detecting very weak He I in the earliest O-type stars.

2.3. Photometry and Transformation Issues

Most of our stars were present in the *HST* ACS/HRC field of view (Figure 2) and this is our primary source for the photometry. The images we analyzed had been taken through the F435W and F550M filters, similar to Johnson B and V (but see below). Each image consisted of four dithered exposures (offset one from another by a fraction of an arcescond), combined into a single "drizzled" image for better sampling of the point-spread function. The scale of the final image is $0\farcs025$ pixel^{-1}. The total integration time for each image was 8 s. The images were taken on 2005 December 29.

For the actual photometry, we used the PHOT application of the DAOPHOT package of IRAF, adopting an aperture radius of 3.0 pixels ($0\farcs08$). We then determined the aperture correction from 3.0 pixels to the ACS "standard" aperture of $0\farcs5$ using a few isolated stars on each frame. We adopted the published aperture correction from $0\farcs5$ to infinity from Sirianni et al. (2005). The counts were corrected for the charge transfer efficiency losses, dependent upon the sky background and position on the chip, following the formulation in Pavlovsky et al. (2006). We note that the CTE correction is quite significant, amounting to −0.01 to −0.07 mag, depending upon the brightness and location of a star.

Although Sirianni et al. (2005) recommend working in the ACS "native" photometric system, we have instead chosen to transform to the standard (Johnson) system. We wish to determine the color excesses and distance modulus to the cluster, and to do this we rely upon our knowledge of the intrinsic colors and absolute magnitudes of O stars as a function of spectral type (see, e.g., Conti et al. 1988; Massey 1998a). These quantities are known *empirically* as the result of observational studies in the standard system rather than through models that can simply be recomputed for some alternative bandpass. In other words, we know that an O7 V star has $(B-V)_0$ of −0.32 and $M_V = -4.9$ through observations of young clusters, not as the result of computations. Thus, in order to compute color excesses and derive spectroscopic parallaxes we need to transform *something*: either we transform the intrinsic colors and absolute magnitudes to the ACS system, or we transform the ACS photometry to the standard system. We have chosen the latter, since (a) this allows us to include stars outside the ACS/HRC field for which standard photometry exists, and (b) it allows us to compare our results to others. That said, we need to emphasize that the transformations introduce uncertainties well beyond the usual photometric errors.

Sirianni et al. (2005) list transformations to B for F435W ACS/HRC photometry, but the transformations are based upon unreddened stars, rather than reddened O stars as is the case here. Furthermore, they offer no transformation for the F550M filter. So, we have determined corrections ourselves as follows. First, we placed the F435W and F550M photometry on the so-called VEGAMAG system using the revisions to the Sirianni et al. (2005) zeropoints listed on the ACS Web site.[8] We then corrected the photometry for the fact that Vega actually does not have zero magnitude, but rather $B = V = +0.03$ (Bessell et al. 1998; see also Maíz Apellániz 2006). Using the Kurucz (1992) Atlas 9 models appropriate for O-type stars ($\log g = 5.0$ and $T_{\rm eff} =$ 40,000, 45,000, and 50,000 K), we then computed F550M − V and (F435W − F550M)−$(B-V)$ for various amounts of reddenings, where we have adopted the Cardelli et al. (1989) Galactic reddening law.

For an O star with reddening in the range we expect for NGC 3603 [i.e., $E(B-V) = 1.3-1.5$], we find F550M−V = −0.11 to −0.12. We adopt F550M−V = −0.11. Similarly we find F435W−B = +0.0 to +0.02, and we adopt F435W−B = +0.01. Thus (F435W− F550M)−$(B-V)$ = +0.12.[9] J. Maíz Apellániz (2007, private communication) derives essentially identical corrections for similarly reddened O stars.

We note that the transformations are sensitive at the 0.02–0.03 mag level to the details of the adopted bandpasses. For the ACS bandpasses, we synthesized an effective bandpasses using SYNPHOT, which includes the wavelength-dependent sensitivities of the entire system (telescope + filter + instrument). Historically, knowledge of the standard Johnson bandpasses has required some "reverse engineering," tested by using the deduced bandpasses with model atmospheres to reproduce the observed colors of stars (see Buser & Kurucz 1978; Bessell et al. 1998). For B and V, SYNPHOT adopts the bandpasses determined by Maíz Apellániz (2006), which are similar to, but not quite identical to, the Bessell (1990) versions. Using the Bessell (1990) prescriptions would result in a 0.02 mag shift in both the F435W−B and F550M−V transformations used here. Similarly, if we instead adopted the bandpasses determined by Buser & Kurucz (1978), our conversions would differ by 0.03 mag for F435W − B and by 0.01 in F550M − V.

We list the resulting magnitudes and colors in Table 1 as V and $B-V$. It is worth comparing our photometry to that of others, as a check on our transformations. For nine stars in common to Melnick et al. (1989) in our V-band photometry, we exclude two outliers, and then find a mean difference of +0.04 mag, in the sense of our values minus those of Melnick et al. (1989). We identify only three stars in common for which we have $B-V$ values; for these, we find an average difference of −0.02 mag in the same sense. Drissen et al. (1995) list "B" values they derived from just averaging the flux in their spectra from 4000 Å to 4750 Å. The difference for their 13 stars (our values minus theirs) is +0.05 mag.[10] We conclude that our photometry is the best that we can do unless and until well-calibrated exposures can be made under good seeing conditions in filter systems which are a closer approximation to the standard system.

Some stars fell outside the area covered by the HRC image. Although the same *HST* ACS program included images taken with the Wide Field Camera of the ACS, all the stars of interest were quite saturated on these archival images. So, instead, we used a 20 s V-band exposure taken for us by the SMARTS consortium as part of a separate investigation looking for eclipsing binaries in NGC 3603. We used three stars in common to set the photometric zeropoint consistently with the ACS/HRC system. The image was taken on 2006 April 3, and the seeing was $1\farcs4$, and is used for the finding chart in Figure 1. As we lacked a B-band exposure, we adopt the $B-V$ values of Melnick et al. (1989) for those stars, when available. The agreement between the SMARTS data and Melnick et al. (1989) is good, with an average difference of +0.03 mag, again in the

[8] http://www.stsci.edu/hst/acs/analysis/zeropoints.

[9] In contrast, for an *unreddened* O-type star we find F550M−V = +0.0, F435W−B = −0.07 and hence (F435W− F550M)−$(B-V)$ = −0.07.

[10] We exclude the star NGC 3603-33, which both they and we find to be marginally resolved on the *HST* images.

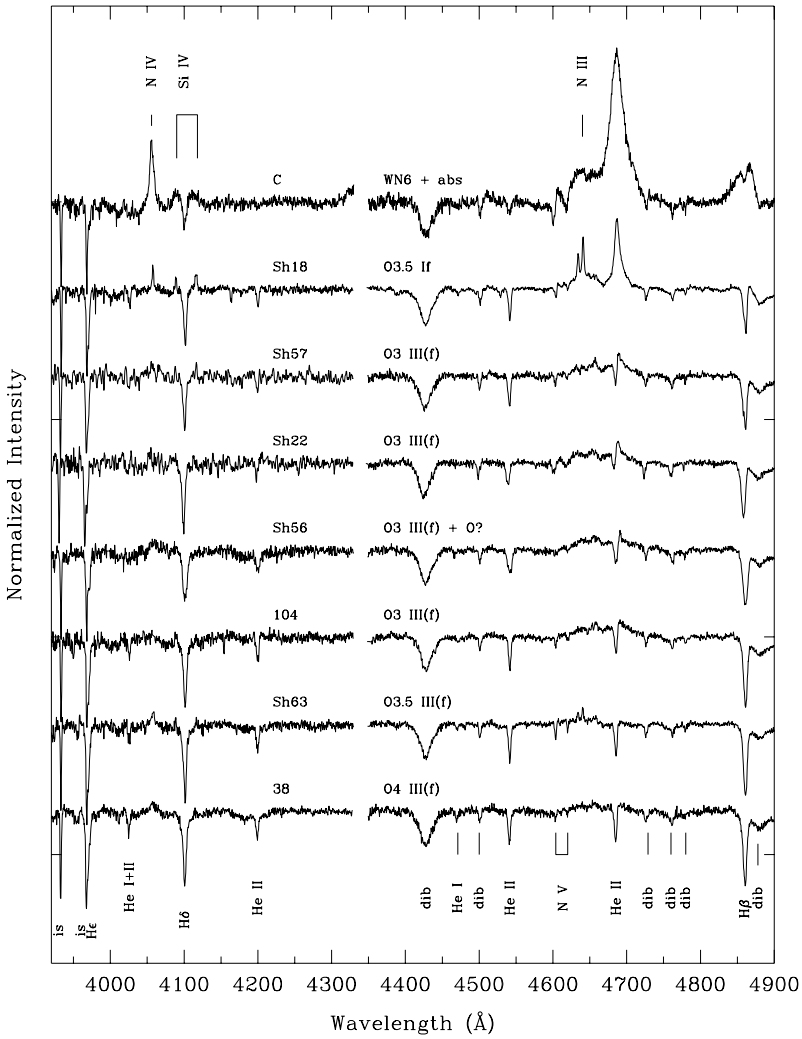

Figure 3. Normalized spectra of NGC 3603 supergiants and giants. Only the data in the blue (MK classification) region are shown. The interstellar (is) H and K Ca II lines and diffuse interstellar bands (DIBs) are marked, along with the prominent stellar features. The displacement between the various spectra is 0.4 times the continuum level.

sense of our values minus theirs. The photometry of the star Sher 58 clearly differs significantly ($\Delta V = 0.58$ mag). Their color of this star leads them to conclude it is not a member, but their value is inconsistent with the O8 V spectral type we find, leading us to suspect that we have identified different stars as Sher 58. The star has a close companion, as is seen in Figure 1.

3. SPECTRAL CLASSIFICATIONS

The spectra were classified two ways. First, a qualitative assessment was made by comparing the observed spectra to those illustrated by Walborn & Fitzpatrick (1990). Second, a more precise determination was then made quantitatively by measuring the equivalent widths (EWs) of He I λ4471 and He II λ4542 and computing $\log W' = \log(\mathrm{EW\ He\,I}/\mathrm{EW\ He\,II})$. The latter has been calibrated against spectral class by Conti (see Conti & Alschuler 1971; Conti 1973; Conti & Frost 1977; see the summary in Conti 1988), and indeed forms the astrophysical basis for the spectral classification of O-type stars. Our experience has shown that the visual method works best on spectra with a low or modest SNR, while the latter is more accurate for data with a high SNR and adequate spectral resolution. In either scheme, the primary diagnostic for the spectral subtypes for O stars is the relative strength of He I and He II, while the primary luminosity indicators are the strength (emission or absorption) of the He II λ4686 line and the presence and strength of the N III λλ4634,42 emission lines. For the earliest O types (O2–O3.5), we also considered the criteria suggested by Walborn et al. (2002), namely the relative strengths of N III and N IV emission, although it has yet to be shown whether or not this defines an extension of the temperature sequence (see the discussion in Massey et al. 2005). We include the new spectral types in Table 1, and illustrate our spectra in Figures 3–6.

In a few cases, it was clear that our spectral extraction apertures contained some light from neighboring objects. If the contamination was judged severe, we did not include the star in our study. However, there were a few cases where there was some minor blending, and we note such cases. For these, the spectral types may not be as good as for the other stars in our sample.

We were able to classify 26 stars in the cluster, 16 of which were previously unclassified. Among these are a number of newly classified O3 and O4 types. We compare our new spectral

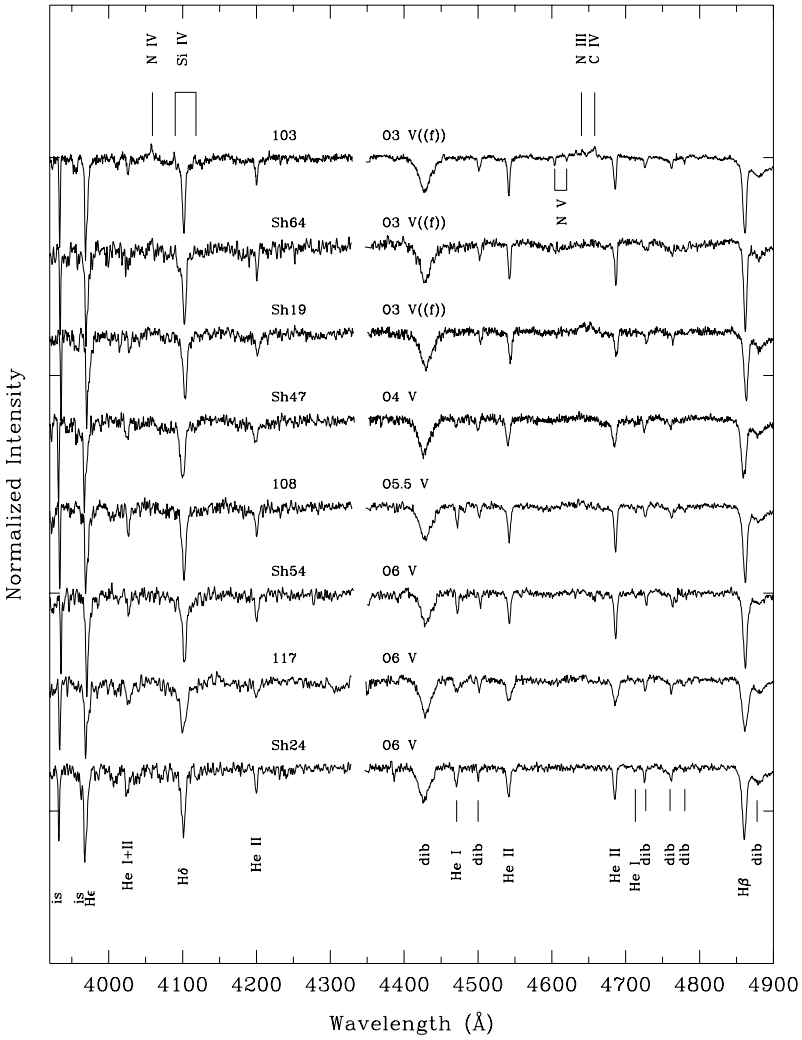

Figure 4. Same as Figure 3 for O3–O6 dwarfs.

types to those in the literature in Table 2. In general, we find very good agreement, usually within a single type and luminosity class. Our experience has shown that nebular contamination can substantially alter the classification, particularly for the early O stars where He I λ4387 is not visible, and one must rely solely on He I λ4471, which may be filled in by nebular emission. In choosing which stars to observe we generally decided not to observe the stars that had been previously observed with the *HST's* FOS by Drissen et al. (1995). Although Drissen et al.'s (1995) sample was observed without the benefits of sky subtraction, the FOS observations were obtained with such a small aperture (0.″25) that nebular contamination should not be an issue. However, we did decide to include a number of stars that had been previously observed by Moffat (1983), as these were observed photographically. Given this, we find the agreement remarkably good, a testament to the careful work of the previous studies. That said, there are a few differences we note in discussing the stars individually.

NGC 3603-Sh27. Our spectrum of this star (Figure 5) is of unusually low SNR, about 130 per 2 Å spectral resolution element. Nevertheless, it is easy to classify as roughly O7 V. We measure an EW of 650 mÅ for He I λ4471, and 600 mÅ for He II λ4542, yielding a $\log W' = +0.0$ and thus an O7.5 type. The lack of He II λ4686 emission makes this a dwarf.

NGC 3603-Sh54. Visually we classified this star as O6 V, with He I λ4471 just a bit weaker than He II λ4542 (Figure 4). We measure 310 mÅ and 520 mÅ, respectively, leading to a $\log W' = -0.23$, also leading to an O6 type (Conti 1988). The strength of He II λ4686 absorption and lack of discernible N III λλ4634,42 emission identifies the star as a dwarf.

NGC 3603-103. The spectrum is shown in Figure 4. This star was slightly blended in our extraction window. We detect extremely weak He I λ4471 absorption in our spectrum (EW = 30 mÅ), typical of the very earliest O-type stars (see Massey et al. 2004, 2005). He II λ4542 has an EW of 660 mÅ, so $\log W' = -1.3$. We call this star an O3 V((f)), where the luminosity designation denotes a dwarf with weak N III λλ4634,42 emission and He II λ4686 in absorption.

NGC 3603-109. Visually the spectrum of this star appears to be of an O7 V, with He I λ4471 a bit weaker than He II λ4542 (Figure 5). We measure EWs of 650 mÅ and 780 mÅ, respectively, or $\log W' = -0.08$. This is consistent with the O7 V designation. The star was slightly blended on the slit.

NGC 3603-Sh63. We show the spectrum of this star in Figure 3. This star has weak He I λ4471, with an EW of about

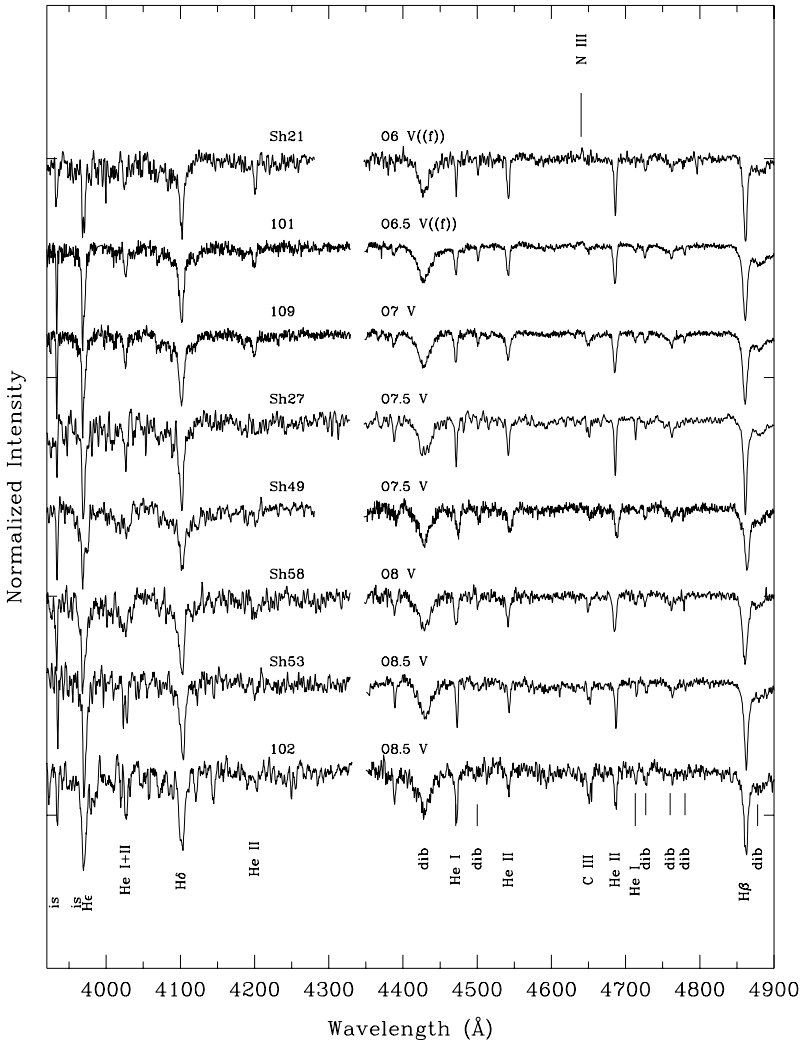

Figure 5. Same as Figure 3 for O6–O8.5 dwarfs, except that the displacement between the spectra is 0.6 times the continuum level.

180 mÅ, a little large for us to consider the star an O3 (i.e., Kudritzki 1980; Simon et al. 1983; see the discussion in Massey et al. 2004, 2005). Yet, N IV λ4058 emission is much stronger than that of N III λλ4534,42 emission, which would make it an O3 by the criteria enumerated by Walborn et al. (2002). In addition, NV λλ4603,19 absorption is stronger than what we would expect for an O4 star. He II λ4542 has an EW of 730 mÅ, and so log $W' = -0.61$, right on the border between O4 and earlier types. In addition to N III λλ4634,42 emission, He II λ4686 is weak with emission wings, and so we call this an O3.5 III(f). Still, NV λλ4603,19 appears to be even a bit too strong for this late classification; possibly the star is composite, although here we will treat it as single. The star was previously classified by Moffat (1983) as considerably later, and of lower luminosity, O5.5 V.

NGC 3603-38. The spectrum of this star is shown in Figure 3. We measure He I λ4471 to have an EW of 120 mÅ, while He II λ4542 has an EW of 590 mÅ, leading to an O4 class (log $W' = -0.69$). There is a little emission at N III λλ4634,42 and He II λ4686 is weak with emission wings, and so we call this an O4 III(f). Previously it was called an O3 V by Drissen et al. (1995). The star was slightly blended on our slit, so it is possible that the Drissen et al. (1995) type is more accurate. We do see what might be weak He I λ4387 and λ4009, due presumably to the slight blend.

NGC 3603-101. Our visual impression of the spectrum of this star places it in the range O6–O7 V type (Figure 5). We measure EWs of 430 mÅ and 580 mÅ for He I λ4471 and He II λ4542, respectively, leading to a log $W' = -0.13$ and an O6.5 type according to Conti (1988). The star is a dwarf, judged from the lack of any emission at He II λ4686. Very weak emission at N III λλ4634,42 may be present, and we have indicated this by adding an "((f))" description to the luminosity class.

NGC 3603-Sh53. Our spectrum of this star is unusually noisy, with an SNR of only 120 per 2 Å spectral resolution element. Nevertheless, its classification is straightforward as it is of mid-O type, with strong He I λ4471 and He II λ4542; the former is stronger (Figure 5). We classify this as an O8.5 V, having measured EWs of 640 mÅ and 380 mÅ, respectively, leading to a log $W' = 0.23$.

NGC 3603-104. The spectrum of this star is shown in Figure 3. He I λ4471 is very weak, with an EW of 50 mÅ, comparable to that seen in other O3 stars (Kudritzki 1980). The EW of He II λ4542 is 600 mÅ, leading to a log $W' = -1.08$. N III

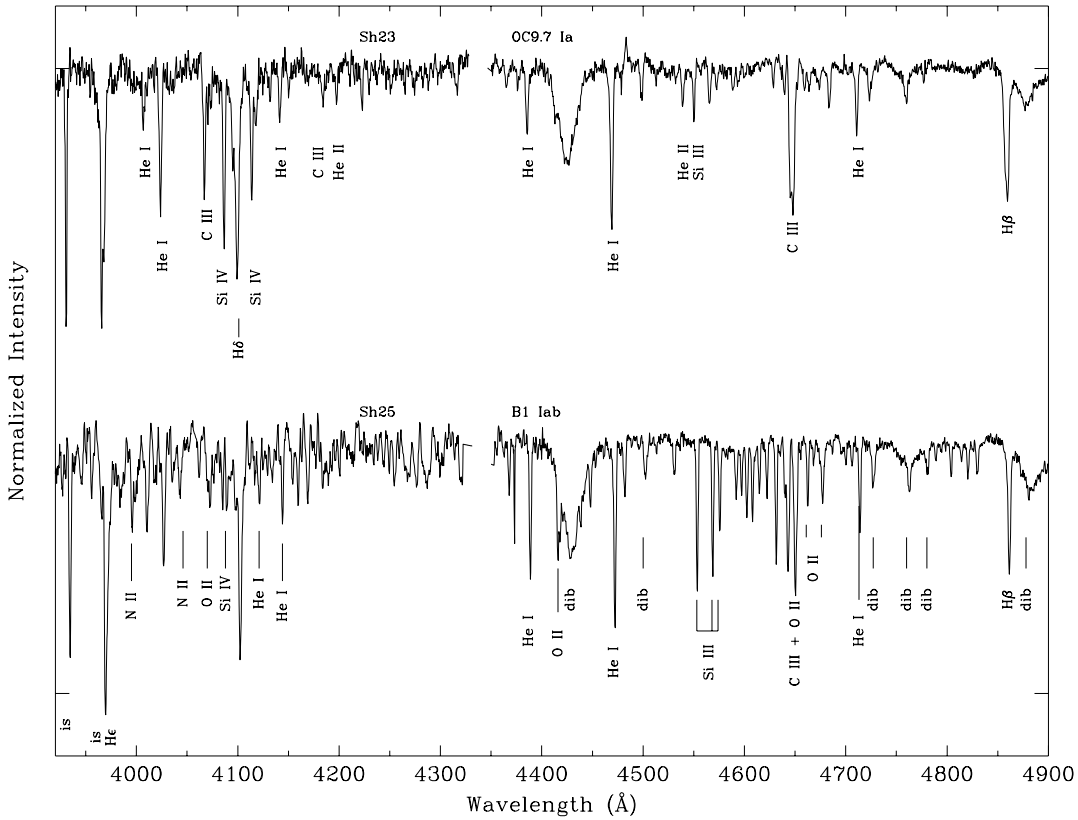

Figure 6. Same as Figure 3 for the two "late-type" supergiants in our sample, an OC9.7 Iab star (Sh 23) and a B1 Iab star (Sh 25). The bluest part of the spectrum in the latter star has been heavily smoothed. The displacement between the two spectra is 0.6 times the continuum level.

λλ4634,42 shows weak emission, and He II λ4686 is weakly in absorption with emission wings, and we call this star an O3 III(f).

NGC 3603-Sh56. The spectrum of this star is shown in Figure 3. This too is a very early O-type star, with He I λ4471 having an EW of 75 mÅ. Thus we expect this star is of O3 type. He II λ4542 has an EW of 750 mÅ, leading to $\log W' = -1.00$, far more negative than the $\log W' = -0.6$ used to separate O4s from later type, and thus consistent with our assigned type. N III λλ4634,42 is weakly in emission, and He II λ4686 has a strong emission component (the line appears to be almost P Cygni), suggesting an O3 III(f). However, there is a hint of double lines in our spectra, and although we cannot say what the spectral type is of the companion, it may be quite early too. We list this spectrum as an O3 III(f)+O? We do not include this star when determining the distance modulus in the next section. Moffat (1983) classified the star a bit later (O4) and of lower luminosity class.

NGC 3603-C. This star shows classic WR features of the WN6 subclass, with strong, broad He II λ4686 emission as well as N III λλ4634,42 and N IV λ4058 emission (Figure 3). There is absorption superimposed on the Balmer/Pickering lines (Hβ and Hδ), as well as at He II λ4542 absorption. We call this WN6+abs, consistent with previous classifications.

NGC 3603-117. The spectrum of this star is shown in Figure 4. The lines in this star are quite wide. The EW of He I λ4471 is 500 mÅ, while that of He II λ4542 is 690 mÅ, but with considerable uncertainty due to the broadness of the lines. With $\log W' = -0.14$, the Conti (1988) criteria would lean to an O6.5 classification. However, the weakness of He I λ4387 and general appearance of the spectra suggest a slightly earlier type. We call the star an O6 V, with the luminosity class reflecting the lack of emission at N III λλ4634,42 and at He II λ4686.

NGC 3603-Sh25. The spectrum is shown in Figure 6. This star has long been known to be an early-type B supergiant; Moffat (1983) classified it as a B1.5 Iab. We would make it just slightly earlier, about B1, based on the relative strengths of Si IV λ4089 and Si III λ4553.

NGC 3603-Sh64. The spectrum of this star is shown in Figure 4. This is a very early O-type star, with He I λ4471 just barely discernible on our spectrum; we measure an EW of about 30 mÅ, making the star O3 (or earlier). He II λ4542 has an EW of 630 mÅ, making $\log W' = -1.3$. The luminosity class V, with weak N III λλ4634,42 emission but strong He II λ4686 absorption. We classify it as an O3 V((f)).

NGC 3603-102. The spectrum of this star is shown in Figure 5. The SNR of our spectrum of this star is only 100 per 2 Å spectral resolution element, but fortunately it is easily classified. We call it an O8.5 V. He I λ4471 has an EW of 950 mÅ, while He II λ4542 has an EW of 530 mÅ, leading to a $\log W' = 0.25$, in agreement with this type. It is a dwarf.

NGC 3603-Sh57. The spectrum of this star is shown in Figure 3. The EW of He I λ4471 is only 30 mÅ, comparable to what Massey et al. (2004, 2005) found in stars as early as O2. He II λ4542 has an EW of 540 mÅ, so $\log W' = -1.3$. Thus the absorption line spectrum of this star suggests that it is O3 or earlier. The strength of N III and He II λ4686 emission makes this a giant. We find that N IV λ4058 emission is comparable to N III λλ4634,42 emission, precluding an O2 classification (Walborn et al. 2002). For giants, Walborn et al. (2002) would require

Table 2
NGC 3603 Stars with Newly Found Spectral Types

Star	New	Literature	
	Spectral Type	Spectral Type	Ref.
Sh27	O7.5 V	...	...
Sh54	O6 V	...	...
103[a]	O3 V((f))	...	...
109[a]	O7 V	...	...
Sh63	O3.5 III(f)	O5.5 V	1
38[a]	O4 III(f)	O3 V	2
101	O6.5 V((f))	...	...
Sh53	O8.5 V	...	...
104	O3 III(f)	...	...
Sh56	O3 III(f)+O?	O4 V(f)	1
C	WN6 + abs	WN6 + abs	2
117	O6 V	...	...
Sh25	B1 Iab	B1.5 Iab	1
Sh64	O3 V((f))	...	...
102	O8.5 V	...	...
Sh57	O3 III(f)	O5 III(f)	1
108[a]	O5.5 V	...	...
Sh18	O3.5 If	O6 If	1
Sh58	O8 V[a]	...	...
Sh24	O6 V	...	...
Sh49	O7.5 V	...	...
Sh47	O4 V	O4 V	1
Sh23	OC9.7 Ia	O9.5 Iab	1
Sh22	O3 III(f)	O5 V(f)	1
Sh21	O6 V((f))	...	...
Sh19	O3 V((f))	...	...

Notes.
[a] Composite?
References. References for spectral types from the literature: (1) Moffat (1983); (2) Drissen et al. (1995).

this fact to result in an O3.5 III(f) classification, but we are not comfortable classifying it this late given the weakness of He I λ4471 absorption, and so we call it an O3 III(f). It was previously called O5 III(f) by Moffat (1983).

NGC 3603-108. The visual impression of this star is that it is roughly O6 V (Figure 4). Measurements of He I λ4471 (EW = 320 mÅ) and He II λ4542 (EW = 800 mÅ) leads to a more precise O5.5 ($\log W' = -0.40$). There is no emission in N III λλ4634,42 or He II λ4686, leading to the dwarf luminosity class. The star was slightly blended with a neighbor on the slit. We see very weak Mg I λ4481 absorption, which is probably due to this blend.

NGC 3603-Sh18. Visually this is a classic O3–O4 If star (Figure 3), closely resembling the spectral standards HD 93129A and HDE 269698 illustrated in Walborn & Fitzpatrick (1990).[11] The strength of N V λλ4603,19 is intermediate between the two. N IV λ4058 emission is weaker than N III λλ4634,42, which would lean the classification toward an O3.5 If–O4 If type by the criteria listed by Walborn et al. (2002). The EW of He I λ4471 is only 50 mÅ, though, while He II λ4542 has an EW of 530 mÅ, leading to $\log W' = -1.0$, making this solidly an O3 type using the criteria suggested by Conti (1988). We compromise with an O3.5 If type. The strong N III λλ4634,42 and He II λ4686 emission leaves no doubt to its luminosity class. The star was previously classified as much later, O6 If, by Moffat (1983). N. Walborn (2007, private communication) reports having independently classified the star O4 If from as-yet unpublished data, in agreement with our own type.

NGC 3603-Sh58. Visually this star is roughly O7–O8 V (Figure 5). We measure nearly equal He I λ4471 (EW = 640 mÅ) and He II λ4542 (EW = 480 mÅ), leading to a $\log W' = +0.13$, corresponding to an O8 class. He II λ4686 is strongly in absorption, and the star is clearly a dwarf. The star was somewhat blended on our extraction aperture, and we find that the He I lines may be broader than the He II lines, suggesting that the resulting type may be a composite. We will therefore exclude it when computing the distance modulus in the next section. Melnick et al. (1989) listed this star as a non-member (their No. 30) based upon their measurement of a very blue color for the star ($B - V = 0.47$), quite unlike the heavily reddened O stars members. However, our photometry gives a color similar to that of the other O stars, and a spectral type that confirms membership.

NGC 3603-Sh24. Visually this star is an O6 V (Figure 4). We measure an EW of 300 mÅ for He I λ4471, and an EW of 610 mÅ for He II λ4542. The resulting value $\log W' = -0.31$ is borderline between an O5.5 and an O6, and we retain the O6 V classification. The strength of He II λ4686 absorption makes this a dwarf.

NGC 3603-Sh49. Our visual impression of the spectral type of this star is that of an O8 V (Figure 5). We measure an EW of He I λ4471 of 570 mÅ, and an EW of He II λ4542 of 560 mÅ, essentially identical, leading us to an O7.5 V type.

NGC 3603-Sh47. This is another early-type O star (Figure 4), with weak He I (EW of 90 mÅ). He II λ4542 has an EW of 650 mÅ, and thus $\log W' = -0.86$, making the star O4 or earlier by Conti (1988). There is only very weak N III λλ4638,42 emission, and He II λ4686 is in absorption. The star has previously been called an O4 V by Moffat (1983), and we retain this type.

NGC 3603-Sh23. This is a late-type O supergiant (Figure 6). The star closely matches the spectra of HD 152424 and HD 104565 shown by Walborn & Fitzpatrick (1990), and we thus classify the star as an OC9.7 Ia, where the "C" denotes the excessively strong C III λ4650 line. This is in substantial agreement with the O9.5 Iab type found by Moffat (1983).

NGC 3603-Sh22. This is clearly a very early O-type star (Figure 3). Despite a SNR of >350 per spectral resolution element, we detect *no* He I λ4471. The EW must be <20 mÅ. N IV λ4058 and N III λλ4634,42 emission are both weak, but unfortunately the N IV line also coincides with some bad pixels. We call the star an O3 III(f), although it could be an O2 by the Walborn et al. (2002) criteria. The giant luminosity class comes about from the modest emission at He II λ4686. The star had been called an O5 V (f) by Moffat (1983).

NGC 3603-Sh21. The spectrum of this star is shown in Figure 5. Our initial impression of the spectrum of this star is that it is roughly of type O6 V, with He I a bit weaker than He II. We measure EWs of 390 mÅ and 700 mÅ, respectively, leading to a value $\log W' = -0.25$, consistent with the O6 class.

NGC 3603-Sh19. The spectrum of this star is shown in Figure 4. This is another very early O star. Our spectrum has a fairly low SNR (200 per 2 Å resolution element) and we detect *no* He I. We call this an O3 V((f)).

4. RESULTS

We are now prepared to derive values for the reddening, distance, and age of the NGC 3603 spectroscopic sample. We

[11] Walborn et al. (2002) use HD 93129A now as an example of the O2 If type.

Table 3
Reddening, Distances, and Absolute Magnitudes

Star	V	$B-V$	Spectral Type	$E(B-V)$	Adopted M_V[a]	$V-M_V$	Computed M_V[b]	$\log T_{\rm eff}$	$M_{\rm bol}$
Sh27	15.04	1.05	O7.5 V	1.37	−5.0	20.04	−4.0	4.541	−7.3
Sh54	14.57	1.08	O6 V	1.40	−5.1	19.67	−4.6	4.583	−8.2
103	13.09	0.99	O3 V((f))	1.31	−5.4	18.49	−5.7	4.667	−9.9
109	13.85	0.99	O7 V	1.31	−4.9	18.75	−4.9	4.556	−8.4
Sh63	13.41	1.04	O3.5 III(f)	1.37	−5.9	19.31	−5.6	4.653	−9.7
38	13.21	0.97	O4 III(f)	1.30	−6.0	19.21	−5.5	4.643	−9.5
45	14.14	1.00	O8 V− III	1.32	−4.8	18.94	−4.7	4.528	−7.9
41	14.24	1.00	O4 V	1.32	−5.8	20.04	−4.6	4.643	−8.6
42	12.99	1.03	O3 III(f*)	1.36	−5.8	18.79	−6.0	4.667	−10.2
101	14.02	1.08	O6.5 V((f))	1.40	−5.1	19.12	−5.1	4.568	−8.7
36	14.52	0.99	O6 V	1.31	−5.1	19.62	−4.2	4.583	−7.9
40	13.33	1.05	O3 V	1.37	−5.4	18.73	−5.7	4.667	−9.9
Sh53	14.47	1.12	O8.5 V	1.43	−4.9	19.37	−4.8	4.515	−8.0
104	13.02	1.06	O3 III(f)	1.39	−5.8	18.82	−6.1	4.667	−10.3
A2	12.53	1.04	O3 V	1.36	−5.4	17.93	−6.4	4.667	−10.7
A3	13.09	1.04	O3 III(f*)	1.37	−5.8	18.89	−5.9	4.667	−10.1
117	14.17	1.10	O6 V	1.42	−5.1	19.27	−5.1	4.583	−8.7
Sh25	12.23	1.42	B1 Iab	1.60	−6.5	18.73	−7.8	4.342	−9.7
Sh64	13.58	1.15	O3 V((f))	1.47	−5.4	18.98	−5.9	4.667	−10.1
16	13.53	1.08	O3 V	1.40	−5.4	18.93	−5.6	4.667	−9.8
102	15.32	1.10	O8.5 V	1.41	−4.9	20.22	−3.9	4.515	−7.0
Sh57	13.28	1.06	O3 III(f)	1.39	−5.8	19.08	−5.8	4.667	−10.0
108	13.71	1.10	O5.5 V	1.42	−5.2	18.91	−5.5	4.597	−9.2
Sh18	12.65	1.21	O3.5 If	1.53	−6.3	18.95	−7.1	4.597	−10.8
Sh24	14.27	1.11	O6 V	1.43	−5.1	19.37	−5.0	4.583	−8.6
Sh49	14.67	1.10	O7.5 V	1.42	−5.0	19.67	−4.6	4.541	−7.9
Sh47	12.72	1.14	O4 V	1.47	−5.8	18.52	−6.7	4.643	−10.8
Sh23	12.70	1.14	OC9.7 Ia	1.39	−6.0	18.70	−6.4	4.481	−9.3
Sh22	13.21	1.06	O3 III(f)	1.39	−5.8	19.01	−5.9	4.667	−10.1
Sh21	14.75	1.12	O6 V((f))	1.44	−5.1	19.85	−4.6	4.583	−8.2
Sh19	13.65	1.02	O3 V((f))	1.35	−5.4	19.05	−5.3	4.667	−9.5

Notes.
[a] From spectral type and luminosity class.
[b] Computed using our apparent spectroscopic distance modulus corrected by $4.3 \times [E(B-V) - 1.39]$.

begin with the reddenings. In Table 3, we include the values of $E(B-V)$ we derive, using the intrinsic colors of Table 3 from Massey (1998a), and the observed colors from Table 1.

We derive an average reddening $E(B-V) = 1.394 \pm 0.012$ (standard deviation of the mean, hereafter "s.d.m."). The median is 1.39. This is very similar to Moffat's (1983) finding of an average value of $E(B-V) = 1.44$. Sung & Bessell (2004) find a somewhat lower value, $E(B-V) = 1.25$, in the core of the cluster, but argue that it increases to larger values at greater distances. Moffat (1983) noted that there was very little spread in the reddening among the cluster stars—his sample showed a dispersion of only 0.09 mag. We find an even smaller dispersion, 0.06 mag. We are thus reassured that the reddening is well determined to the O stars in NGC 3603, and agree with the conclusion of Moffat (1983) that there is very little variation in reddening across this cluster. We adopt an average value of $E(B-V) = 1.39$.

It is interesting to note that the B1 supergiant, Sher 25, has a color excess that is considerably larger than average. This supergiant has been compared to the progenitor of SN 1987A (see Smith 2007; Smartt et al. 2002), and is known to show circumstellar material (Brandner et al. 1997).

Next, let us derive a distance modulus to the cluster by adopting an absolute magnitude for each star based upon the spectral type and luminosity class. We adopt the values of Conti et al. (1983) for the O stars, interpolating as needed; for the B supergiant (Sher 25), we adopt $M_V = -6.5$ from Humphreys & McElroy (1984). If we make *no* correction for the reddening to the cluster, we derive an *apparent* distance modulus of 19.12 ± 0.09 (s.d.m.). The standard deviation of this sample is 0.5 mag, which is what we expect, given that that is also the typical scatter in M_V for a given spectral type and luminosity class (Conti 1988). The median is 19.00. If we exclude the giants and supergiants (as their absolute magnitudes might cover a larger range), we determine similar values: the average is 19.21 ± 0.12 (s.d.m.), with a standard deviation of the sample of 0.6 mag. The median is 19.07. We therefore adopt an *apparent* distance modulus to the cluster of 19.1 ± 0.1.

If the extinction were normal ($R_V = 3.1$) this would then correspond to a true distance modulus of 14.8, or 9.1 kpc. However, Pandey et al. (2000) have investigated the reddening toward this cluster, and conclude that the reddening is anomalously high within, with a ratio of total to selective extinction $R_V = 4.3$, a value that is more typical of dense environments (see, e.g., Whittet 2003). They correct for reddening assuming an $E(B-V) = 1.1$ for foreground (with $R_V = 3.1$), and $R_V = 4.3$ for the color excess above this value; i.e., $A_V = 3.41 + 4.3[E(B-V) - 1.1]$. If we were to make this correction, then the true distance modulus we would obtain would be 14.4, or 7.6 kpc.

Table 4
Stellar Distances to NGC 3603

Study	Method	$E(B-V)$	Adopted R_V	Apparent DM[a] (mags)	Distance (kpc)
Sher (1965)	Main-sequence fitting	1.42	3.0	17.0	3.5
Moffat (1974)	Main-sequence fitting	1.32	3.1	18.7	8.1
Melnick & Grosbol (1982)	Main-sequence fitting	1.38	3.1	17.9	5.3
Moffat (1983)	Spectroscopic parallax	1.44	3.2	18.8	7.0 ± 0.5
Melnick et al. (1989)	Main-sequence fitting	1.44	3.2	18.9	7.2
Crowther & Dessart (1998)	Spectroscopic parallax	1.23	3.2	18.8	10.1
Pandey et al. (2000)	Main-sequence fitting	1.48	3.1/4.3[b]	19.0	6.3 ± 0.6
Sagar et al. (2001)	Spectroscopic parallax	1.44	3.1	18.8	7.2 ± 1.2
Sung & Bessell (2004)	Main-sequence fitting	1.25[c]	3.55	18.6	6.9 ± 0.6
This study	Spectroscopic parallax	1.39	3.1/4.3[b]	19.1	7.6

Notes.
[a] Apparent distance modulus computed using the quoted true distance modulus and the reddening correction made in each study.
[b] A normal R_V of 3.1 is applied for the foreground reddening $E(B-V) = 1.1$, with a value of R_V applied to extinction within the cluster, i.e., $A_V = 3.1 \times 1.1 + [(E(B-V) - 1.1) \times 4.3]$.
[c] For the central cluster.

Table 5
Kinematic Distances to NGC 3603

Study	Distance (kpc)
Goss & Radhakrishnan (1969)	7.1[a]
van den Bergh (1978)	6.8 ± 0.9[a]
De Pree et al. (1999)	7.0[b]
Russeil (2003)	7.9

Notes.
[a] Corrected to $R_0 = 8.5$ kpc.
[b] De Pree et al. (1999) quote a value of 6.1, but one of the co-authors, W. M. Goss (2007, private communication), writes that the value was a mistake, and recomputes a value of 7.0 kpc.

The physical distance to NGC 3603 is poorly determined. There are three methods that have been employed: main-sequence fitting, spectroscopic parallaxes, and kinematic distance determinations based upon rotation models of the Milky Way. We summarize the results in Tables 4 and 5. Main-sequence fitting (Melnick et al. 1989; Pandey et al. 2000; Sung & Bessell 2004) is probably the least certain of these for such a young cluster, given that the theoretical zero-age main-sequence is nearly vertical in the color–magnitude diagram. This is particularly true in the $V - I$ plane used by Sung & Bessell (2004); see their Figure 9. This problem was recognized by van den Bergh (1978), who obtained *UBV* photometry of cluster members, but noted that such data were not sufficient to determine a reliable distance. (He did, however, determine a kinematic distance, as discussed below.) See also the discussion in Sagar et al. (2001). The spectroscopic parallaxes (Moffat 1983; Crowther & Dessart 1998; Sagar et al. 2001) should be more reliable. Our sample of stars is considerably larger than those previously employed. Of course, a key issue in deriving the physical distance is how reddening is treated. In Table 4, we include the *apparent* distance moduli as well as the derived physical distances. We can see that most modern studies derive a similar value for the apparent distance modulus (i.e., 18.6–19.1), despite the extremely large range in physical distances derived (6.3 kpc to 10.1 kpc).

We can compare our distance to the kinematic distances (Table 5). Goss & Radhakrishnan (1969) find a distance of 8.4 kpc, but that was based upon the old assumption that the distance from the Galactic center to the sun is 10 kpc. Correcting to the more modern value $R_0 = 8.5$ kpc would result in a 7.1 kpc distance. Van den Bergh (1978) also derives a similar kinematic distance, 6.8 kpc, when corrected to $R_0 = 8.5$ kpc. De Pree et al. (1999) quote a value of 6.1 ± 0.6 kpc, but one of the co-authors, W. M. Goss (2007, private communication), writes that this value should be revised to 7.0 kpc. Russeil (2003) finds a slightly larger kinematic distance, 7.9 kpc. While these span a range, we can conclude that our apparent distance modulus can be reconciled with the kinematic distance moduli in the literature only if the extinction is anomalous within the cluster, as Pandey et al. (2000) argue.[12]

For constructing the H–R diagram, we have chosen to adopt our *apparent* distance modulus, and then correct individual stars for differences in the average reddening by $4.3 \times \Delta E(B-V)$, where $\Delta E(B-V)$ is the difference between the average color excess 1.39 and that for an individual star. Since the variation in the reddening is small, using 3.1 instead would lead to at most a difference of 0.25 mag in the final value. We include the absolute visual magnitudes obtained by this method in Table 3. In most cases, the agreement between M_V (based on the spectral type and luminosity class) and that computed from the average apparent distance modulus (corrected for reddening above or below the cluster average) is good, within the 0.5 mag scatter we expect (Conti 1988).

Finally, let us use the recent effective temperature scale of Massey et al. (2005) to place these stars on the H–R diagram. The new scale includes the effects of line- and wind-blanketing, which significantly lowers the effective temperatures for Galactic stars. For the B1 I star (Sh 25), we adopted an effective temperature of 22,000 K, consistent with the modeling of Smartt et al. (2002) and the recent findings of Crowther et al. (2006). For that star, we have adopted a bolometric correction of −2.0 mag, also consistent with these studies. We have included

[12] Smartt et al. (2002) reject $R_V = 4.3$ for Sher 25 based on the argument that applying it leads to too high a luminosity for this star, and instead adopt $R_V = 3.7$ on somewhat arbitrary grounds. However, they had (mis)applied $R_V = 4.3$ to the entire line-of-sight reddening ($E(B-V) = 1.60$), rather than applying $R_V = 3.1$ to the foreground reddening ($E(B-V) = 1.1$) and $R_V = 4.3$ to the remainder ($\Delta E(B-V) = 1.60 - 1.10$). Thus, using the Pandey et al. (2000) reddening leads to $A_V = 5.56$ mag, not 6.88 mag, and actually smaller than the value Smartt et al. (2002) adopt ($A_V = 3.7 \times 1.60 = 5.92$ mag).

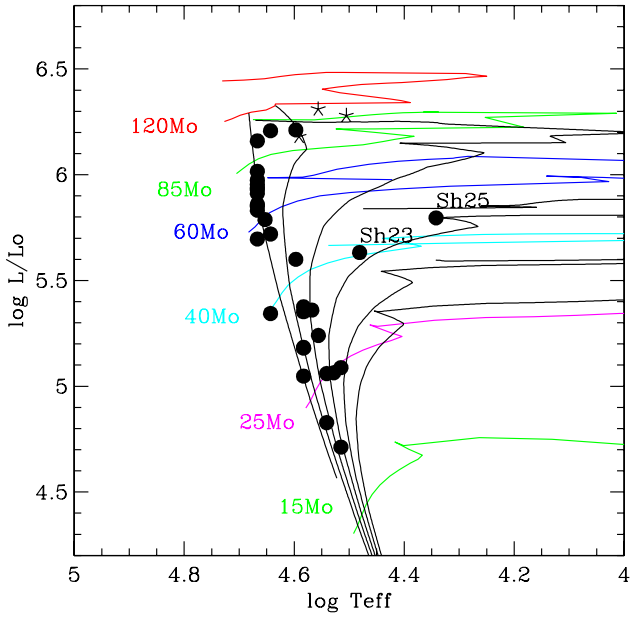

Figure 7. The H–R diagram for NGC 3603. Solid points show the location of the stars listed in Table 3. The non-rotating evolutionary $z = 0.020$ tracks of Schaller et al. (1992) are shown, with the initial masses labeled, in various colors. Isochrones are shown as black curves for 1, 2, 3, 4, 5, and 6 Myr. We have labeled the locations of the OC9.7 Ia star Sh23, and the B1 Iab star Sh 25. The three asterisks denote the location of the three H-rich Wolf–Rayet stars, with the physical properties taken from Crowther & Dessart (1998).

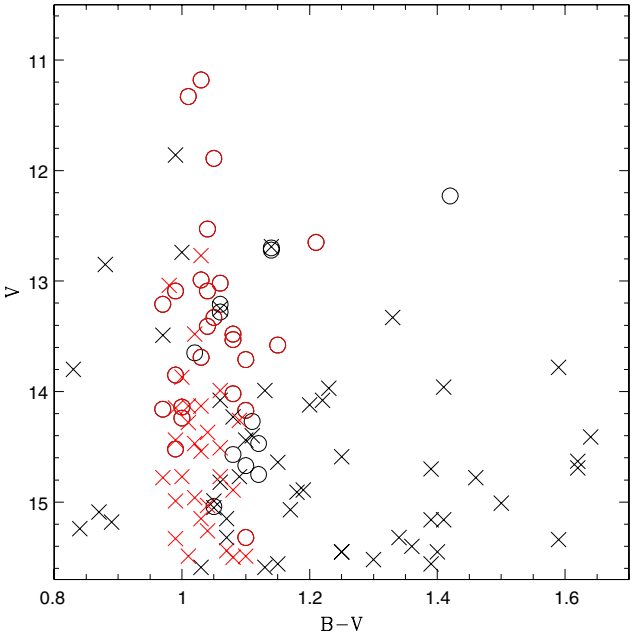

Figure 8. The color–magnitude diagram for NGC 3603. Open circles denote the stars for which there are spectral types; crosses denote the stars for which there are only photometry. Red indicates the stars in the central region (i.e., that covered in Figure 2), and are based upon point-spread function fitting to stars on the HRC images. (This photometry will be fully presented in a later paper.) Black indicates photometry of stars outside the central region, from Melnick et al. (1989).

the three WR stars based upon the modeling of Crowther & Dessart (1998), where we have increased the luminosity by 0.12 dex for consistency with the larger apparent distance modulus found here. We show the resulting H–R diagram in Figure 7. We compare these to the Schaller et al. (1992) evolutionary tracks, which correspond to "Galactic" (solar) metallicity ($z = 0.020$), which is appropriate for NGC 3603 (Smartt et al. 2002; Peimbert et al. 2007; Lebouteiller et al. 2008). The black solid lines denote the isochrones at 1 Myr intervals from an age of 1–6 Myr[13].

First, we see that the masses range above 120 $M_\odot$. We see that the most massive stars are the stars with Wolf–Rayet features analyzed by Crowther & Dessart (1998). In this context, it is worth remembering that in the R136 cluster there were several H-rich WN6 stars which had absorption lines; Massey & Hunter (1998) concluded that these were not evolved objects, but rather "Of stars on steroids," i.e., stars whose masses were so high, and which were so luminous, that their winds were so strong that their spectra simply *resembled* WR stars in having strong emission lines. The modeling of Crowther & Dessart (1998) bears this out: the WRs are coeval with the rest of the cluster, and are simply slightly more luminous and massive. (Note that for simplicity we have truncated the evolutionary tracks prior to the Wolf–Rayet stage.) The most massive non-WR stars in R136 are more massive than we see here but, as discussed below, that could be a metallicity effect. In any event, the unevolved stellar population of NGC 3603 is certainly quite massive.

Secondly, the ages of the highest mass stars are roughly 1–2 Myr, with very little dispersion. Sung & Bessell (2004) obtained a similar result. Stars of somewhat lower mass (<40 $M_\odot$) show a larger dispersion in age, with ages ranging from 1 to 4 Myr. The evolved B-type supergiant Sh 25 and the OC9.7 star Sh 23 have an age of about 4 Myr. This is similar to the age found for stars in the outer regions of the cluster by Sung & Bessell (2004).

It is premature to attempt to derive an initial-mass function for the high-mass stars of NGC 3603, as photometry alone cannot provide a sufficiently accurate discriminant of bolometric luminosity (and hence mass) at such high effective temperatures. (See the discussion in Massey 1998a, 1998b.) Sagar et al. (2001) and Sung & Bessell (2004) do use their deep photometry to compute IMFs for the intermediate-mass stars, but for these photometry does provide a good discriminant. In Figure 8, we show the color–magnitude diagram of the cluster, where we have indicated the stars for which there are spectral types by open circles. We have cut the diagram at $V = 15.6$, corresponding to a ZAMS 20 $M_\odot$ star. (Such a star would have $M_V = 3.5$ and would correspond to a late O-type near the ZAMS.) The photometry for the general field (shown in black) comes from Melnick et al. (1989), while that of the central field (shown in red) comes from the HRC image. We see that, although we have made significant progress in the spectroscopy of stars in NGC 3603, much work remains to be done. In the area outside the core, there are spectra for about 20% of the interesting stars ($V < 15.6$ with colors indicating likely membership), while in the central portion we have spectra for about a third of the stars with $V < 15.6$. (Note that all of the stars in the core have colors indicative of membership.) In all, spectra of another 90

[13] We have used the older Geneva evolutionary tracks of Schaller et al. (1992), rather than the newer ones of Meynet & Maeder (2003), simply for convenience, as Georges Meynet had kindly made available software to compute isochrones from the older tracks. The primary difference with the newer tracks is the inclusion of rotation. While rotation significantly alters the tracks of low-metallicity stars, such as those in the SMC and the LMC, there is much less of an effect at Galactic metallicities; see Meynet & Maeder (2000). We have also truncated the tracks at the start of the WR stage just for clarity.

stars would be needed for a complete census down to 20 $M_{\odot}$. In the central region, observing the majority of the remaining stars will be difficult due to crowding, but not impossible. We hope to undertake such work during the next observing season.

5. DISCUSSION AND SUMMARY

It is worth comparing what we now know about the massive star content of NGC 3603 with that known about the R136 cluster at the heart of the giant H II region 30 Doradus in the LMC. Spectroscopy of the stars in R136 is similarly complete (Massey & Hunter 1998). R136 contains an even greater wealth of O3 stars, and stars extending up to 150 $M_{\odot}$, about the point where the IMF peters out to a single star. In the H–R diagram shown by Massey & Hunter (1998), most of the massive stars appear to be strictly coeval, with an age between 1 and 2 Myr, just as we find here for NGC 3603. For stars with masses below about 40 $M_{\odot}$ the placement of stars in the H–R diagram of R136 was constrained only by photometry, and so there is an (apparent) spread in ages from 0 to 6 Myr, although the actual degree of coevality may be higher. There is a single B-type supergiant in their H–R diagram with a mass of about 20 $M_{\odot}$, and an age of 10 Myr. Maybe that star is an interloper from the field of the LMC, or it could be that in both NGC 3603 and in R136 we simply see that a couple of high-mass stars formed a bit earlier than the majority of stars in the cluster.

We note that both of these clusters contain H-rich WN+abs stars. Massey & Hunter (1998) argued that these were *unevolved* (i.e., core H-burning) stars of high luminosity and mass, whose spectra mimicked that of WN stars given the strong stellar winds expected from high luminosity. Given the ages of the high-mass stars in NGC 3603 or in R136, it is not possible for the WR stars to be evolved (core He-burning) objects, not if they are coeval with the rest of the massive stars. The physical properties of these stars determined by modeling by Crowther & Dessart (1998) are consistent with this.[14] At Galactic metallicity, we would expect the onset of such features to happen at lower mass than in the LMC, so these "Of stars on steroids" in NGC 3603 may be less massive than in the R136 cluster.

We can compare the stellar content straightforwardly. Let us simply count the number of stars with known spectroscopy brighter than a certain bolometric luminosity, $M_{\rm bol} \sim -10$. (For these, our spectroscopy is mostly complete; ($V \sim 13$–13.5; see Figure 8). From Table 3, we find nine stars listed in NGC 3603-12, if we then include the WN+abs stars in the tally. There are perhaps another six stars that have not been observed spectroscopically that could be as bolometrically luminous, so the total is 12–18. In R136, we find 20–29 such stars, depending upon the adopted temperature scale (i.e., Table 3 of Massey & Hunter 1998). So, while R136 is richer in massive stars than NGC 3603, it is only by a factor of 1.1–2.4. Moffat et al. (1994) have also argued for the similarity of the central clusters, suggesting that the primary difference is that NGC 3603 lacks a surrounding massive halo of cluster stars.

In summary, we have obtained spectra of 26 stars in the NGC 3603 cluster, 16 of which have no previous spectroscopy. That brings the total number of stars with spectral types to 38 (Table 1). In addition, we provide identification and ACS/HRC photometry of another 12 stars in the central core for which spectroscopy would be desirable. Our spectroscopic sample includes many stars of type O3. We find an average reddening $E(B-V) = 1.39$, with very little scatter (sample standard deviation of 0.05 mag), indicative of very little variation in reddening in the core. Our spectroscopic parallax for the cluster can be reconciled with the kinematic distance of the cluster if we adopt the reddening proposed by Pandey et al. (2000); we then derive a distance of 7.6 kpc. We emphasize that although there has been a very large range of physical distances derived for this cluster in the past 10 years (6.3–10.1 kpc), there is excellent agreement in the *apparent* distance modulus of the cluster (18.6–19.1 mag). The disagreement in the distances is really based upon exactly how to correct for reddening. We sidestep the issue by using the apparent distance modulus (plus a modest correction for differential reddening) to construct the H–R diagram. It reveals a mostly coeval population of massive stars extending beyond 120 $M_{\odot}$, with ages of 1–2 Myr. The most massive and luminous stars are the H-rich WN stars, as expected by analogy with R136 (Massey & Hunter 1998). Some stars of 20–40 $M_{\odot}$ may show a larger age spread, up to 4 Myr, with the OC9.7 and B-type supergiants having an age of 4 Myr.

Additional spectroscopy of stars is underway by A. F. J. Moffat (2007, private communication), which will further help refine our view of this interesting cluster. While further *HST* STIS spectroscopy of the most crowded members would be highly desirable, it is worth noting how much can now be accomplished from the ground using the best modern telescopes. More such work is needed for deriving an initial-mass function for the massive stars in this cluster, as less than a third of the stars with masses above 20 $M_{\odot}$ have spectroscopy. We hope to help improve this situation in the coming observing season ourselves.

We are grateful to David Osip for allowing us to observe during some Magellan engineering time shortly in advance of our scheduled night. Jesús Maíz Apellániz was kind enough to allow us access to one of the ACS/HRC frames prior to it becoming public in order to prepare for the observing run; we also gratefully acknowledge his calling our attention to an error we made in the photometric transformations in an earlier version of the manuscript. Jennifer Mack provided guidance in our use of SYNPHOT. We also benefited from correspondence with Geoff Clayton, Miller Goss, Tony Moffat, Brian Skiff, and Nolan Walborn, as well as from comments on an early draft by Deidre Hunter. Suggestions by the referee, Stephen Smartt, were useful in improving the paper. N.W.M. and P.M.'s work was supported through the National Science Foundation (NSF) AST-0604569. A.M.Z.'s work was supported through an NSF REU grant, AST-0453611.

[14] These stars were found to be *chemically* evolved, in the sense of showing enhanced CNO products at the surface, but this is still consistent with these being H-burning objects.

REFERENCES

Brandner, W., Grebel, E. K., Chu, Y.-H., & Weis, K. 1997, ApJ, 475, L45
Bessell, M. S. 1990, PASP, 102, 1181
Bessell, M. S., Castelli, F., & Plez, B. 1998, A&A, 333, 231
Buser, R., & Kurucz, R. L. 1978, A&A, 70, 555
Cardelli, J. A., Clayton, G. C., & Mathis, J. S. 1989, ApJ, 345, 245
Conti, P. S. 1973, ApJ, 179, 181
Conti, P. S. 1988, in O Stars and Wolf–Rayet Stars, ed. P. S. Conti, & A. B. Underhill (Washington, DC: NASA SP-497)
Conti, P. S., & Alschuler, W. R. 1971, ApJ, 170, 325
Conti, P. S., & Frost, S. A. 1977, ApJ, 212, 728
Conti, P. S., Garmany, C. D., de Loore, C., & Vanbeveren, D. 1983, ApJ, 274, 302
Crowther, P. A., & Dessart, L. 1998, MNRAS, 296, 622
Crowther, P. A., Lennon, D. J., & Walborn, N. R. 2006, A&A, 446, 279

De Pree, C., G., Nysewander, M. C., & Goss, W. M. 1999, AJ, 117, 2903
Drissen, L., Moffat, A. F. J., Walborn, N. R., & Shara, M. M. 1995, AJ, 110, 2235
Eisenhauer, F., Quirrenbach, A., Zinnecker, H., & Genzel, R. 1998, ApJ, 498, 278
Goss, W. M., & Radhakrishnan, V. 1969, Astrophys. Lett., 4, 199
Harayama, Y., Eisenhauer, F., & Martins, F. 2008, ApJ, in press (arXiv:0710.2882v2)
Humphreys, R. M., & McElroy, D. B. 1984, ApJ, 565
Hunter, D. A., O'Neil, E. J., Lynds, R., Shaya, E. J., Groth, E., & Holtzman, J. A. 1996, ApJ, 459, L27
Kudritzki, R. P. 1980, A&A, 85, 174
Kurucz, R. 1992, in The Stellar Populations of Galaxies, ed. B. Barbuy, & A. Renzini (Dodrecht: Kluwer), 225
Lebouteiller, V., Bernard-Salas, J., Brandl, B., Whelan, D., Wu, Y., Chamandaris, V., & Devost, D. 2008, ApJ, submitted (arXiv:0710.4549)
Maíz Apellániz, J. 2006, AJ, 131, 1184
Massey, P. 1998a, in Stellar Astrophysics for the Local Group, ed. A. Aparicio, A. Herrero, & F. Sanchez (Cambrdige, MA: Cambridge Univ. Press), 95
Massey, P. 1998b, in ASP Conf. Ser. 142, The Stellar Initial Mass Function, 38th Herstmonceux Conference, ed. G. Gilmore, & D. Howell (San Francisco, CA: ASP), 17
Massey, P., Bresolin, F., Kudritzki, R. P., Puls, J., & Pauldrach, A. W. A. 2004, ApJ, 608, 1001
Massey, P., & Hunter, D. A. 1998, ApJ, 493, 180
Massey, P., Puls, J., Pauldrach, A. W. A., Bresolin, F., Kudritzki, R. P., & Simon, T. 2005, ApJ, 627, 477 ApJ, 634, 1286
Melnick, J., & Grosbol, P. 1982, A&A, 107, 23
Melnick, J., Tapia, M., & Terlevich, R. 1989, A&A, 213, 89
Meynet, G., & Maeder, A. 2000, A&A, 361, 101
Meynet, G., & Maeder, A. 2003, A&A, 404, 975
Moffat, A. F. J. 1974, A&A, 35, 315
Moffat, A. F. J. 1983, A&A, 124, 273
Moffat, A. F. J., Drissen, L., & Shara, M. M. 1994, ApJ, 436, 183
Pandey, A. K., Ogura, K., & Sekiguchi, K. 2000, PASJ, 52, 847
Pavlovsky, C., et al. 2006, ACS Data Handbook, Version 5.0 (Baltimore, MD: STScI)
Peimbert, M., Peimbert, A., Esteban, C., Garcia-Rojas, J., Bresolin, F., Carigi, L., Ruiz, M. T., & Lopez-Sanchez, A. R. 2007, RMxAC, 29, 72
Russeil, D. 2003, A&A, 397, 133
Sagar, R., Munari, U., & de Boer, K. S. 2001, MNRAS, 327, 23
Schaller, G., Schaerer, D., Meynet, G., & Maeder, A. 1992, A&AS, 96, 269
Sher, D. 1965, MNRAS, 129, 237
Simon, K. P., Kudritzki, R. P., Jonas, G., & Rahe, J. 1983, A&A, 125, 34
Sirianni, M., et al. 2005, PASP, 117, 1049
Smith, N. 2007, AJ, 133, 1034
Smartt, S. J., Lennon, D. J., Kudritzki, R. P., Rosales, F., Ryans, R. S. I., & Wright, N. 2002, A&A, 391, 979
Stolte, A., Brandner, W., Brandl, B., Zinnecker, H., & Grebel, E. K. 2004, AJ, 128, 765
Sung, H., & Bessell, M. S. 2004, AJ, 127, 1014
van den Bergh, S. 1978, A&A, 63, 275
Walborn, N. R. 1973, ApJ, 182, L21
Walborn, N. R., et al. 2002, AJ, 123, 2754
Walborn, N. R., & Fitzpatrick, E. L. 1990, PASP, 102, 379
Whittet, D. C. B. 2003, Dust in the Galactic Environment (2nd ed.; Bristol: IOP), 91
Zacharias, N., et al. 2004, AJ, 127, 3043